Journal of Biomedical Optics

BiomedicalOptics.SPIEDigitalLibrary.org

Ferric plasmonic nanoparticles, aptamers, and magnetofluidic chips: toward the development of diagnostic surface-enhanced Raman spectroscopy assays

Haley Marks
Po-Jung Huang
Samuel Mabbott
Duncan Graham
Jun Kameoka
Gerard Coté

SPIE.

Haley Marks, Po-Jung Huang, Samuel Mabbott, Duncan Graham, Jun Kameoka, Gerard Coté, "Ferric plasmonic nanoparticles, aptamers, and magnetofluidic chips: toward the development of diagnostic surface-enhanced Raman spectroscopy assays," *J. Biomed. Opt.* **21**(12), 127005 (2016), doi: 10.1117/1.JBO.21.12.127005.

Ferric plasmonic nanoparticles, aptamers, and magnetofluidic chips: toward the development of diagnostic surface-enhanced Raman spectroscopy assays

Haley Marks,[a,b,*] Po-Jung Huang,[c] Samuel Mabbott,[b] Duncan Graham,[b] Jun Kameoka,[d] and Gerard Coté[a,e]
[a]Texas A&M University, Department of Biomedical Engineering, 101 Bizzell Street, College Station, Texas 77843, United States
[b]University of Strathclyde, Department of Pure and Applied Chemistry, 99 George Street, Glasgow G1 1RD, United Kingdom
[c]Texas A&M University, Department of Materials Science and Engineering, 575 Ross Street, College Station, Texas 77843, United States
[d]Texas A&M University, Department of Electrical and Computer Engineering, 188 Bizzell Street, College Station, Texas 77843, United States
[e]Texas A&M University, Texas A&M Engineering Experiment Station Center for Remote Health Technologies and Systems, Department of Biomedical Engineering, 101 Bizzell Street, College Station, Texas 77843, United States

Abstract. Conjugation of aptamers and their corresponding analytes onto plasmonic nanoparticles mediates the formation of nanoparticle assemblies: molecularly bound nanoclusters that cause a measurable change in the colloid's optical properties. The optimization of a surface-enhanced Raman spectroscopy (SERS) competitive binding assay utilizing plasmonic "target" and magnetic "probe" nanoparticles for the detection of the toxin bisphenol-A (BPA) is presented. These assay nanoclusters were housed inside three types of optofluidic chips patterned with magnetically activated nickel pads, in either a straight or array pattern. Both Fe_2O_3 and Fe_2CoO_4 were compared as potential magnetic cores for the silver-coated probe nanoparticles. We found that the $Ag@Fe_2O_3$ particles were, on average, more uniform in size and more stable than $Ag@Fe_2CoO_4$, whereas the addition of cobalt significantly improved the collection time of particles. Using Raman mapping of the assay housed within the magnetofluidic chips, it was determined that a 1×5 array of 50 μm square nickel pads provided the most uniform SERS enhancement of the assay (coefficient of variation ~25%) within the magnetofluidic chip. Additionally, the packaged assay demonstrated the desired response to BPA, verifying the technology's potential to translate magnetic nanoparticle assays into a user-free optical analysis platform.
© 2016 Society of Photo-Optical Instrumentation Engineers (SPIE) [DOI: 10.1117/1.JBO.21.12.127005]

Keywords: surface-enhanced Raman spectroscopy; aptamer; plasmonic nanoparticles; competitive binding assay; molecular diagnostics.

Paper 160560PR received Aug. 20, 2016; accepted for publication Nov. 17, 2016; published online Dec. 20, 2016.

1 Introduction

There is a tremendous interest and need for analytical and information technologies that can be used to diagnose or monitor a person's condition at the point-of-care. One area, in particular, is the real-time detection of a patient's exposure to environmental causes of disease through the use of point-of-care devices during routine medical visits.[1,2] This is consistent with the expectation stated by Rappaport (2011) that medicine will become increasingly personalized, predictive, and preventive.[3] In contrast to environmental biomonitoring, in this paper, the target is human biomonitoring, which aims to determine the body's burden with certain foreign chemicals such as bisphenol-A (BPA) but could also include polychlorinated biphenyls and phthalates, their metabolites, and/or reaction products.[4]

It is well recognized that surface-enhanced Raman spectroscopy (SERS) active colloidal nanoparticles have been used quite successfully to enhance the Raman cross section of a molecule by factors of 10 to 10^8 or more.[5–8] Furthermore, the SERS signal can be obtained using regular low to medium powered lasers (0.1 mW to 1 W) to excite vibrational transitions in molecules adsorbed on a rough metallic (typically Ag or Au) nanoparticle-coated surface and/or in a colloid solution. However, historically, the lack of reliable techniques for controlling the local nanoscale electromagnetic environment in the vicinity of the molecules of interest has been the fundamental experimental limitation to the further quantification and exploitation of SERS. By controlling and optimizing plasmonic nanoparticle aggregation with high-affinity ligands such as DNA probes, antibodies, or aptamers in response to the presence of an analyte, localized areas of concentrated sensing particles are provided, potentially allowing for more repeatable spectral analyses.

A number of ferric micro- and nanoparticle-based SERS assays exist and have recently been studied for bringing human biomonitoring to the point-of-care.[9–16] Magnetic particles are easy to localize using a permanent magnet placed at the side of a vial, at the bottom of a wellplate, near a microfluidic channel, or alternatively using a controllable embedded solenoid. This provides a simple way to exchange buffers, automate assay steps on chip, and reversibly concentrate or aggregate ferric nano- and microparticles. For example, Jaebum Choo's group has utilized magnetic microbeads (analogous to commercially available TurboBeads) for a wide variety of SERS

*Address all correspondence to: Haley Marks, E-mail: hmarks@tamu.edu

1083-3668/2016/$25.00 © 2016 SPIE

biosensing applications, including one embodiment using aptamer-coated gold nanoparticles (AuNPs) for detecting thrombin,[9] another using a solenoid microfluidic chip for trapping a AuNP competitive binding assay against the anthrax biomarker polyglutamic acid,[10] and an IgG immunoassay using antibody-coated hollow gold nanoparticles.[11] While these assays were successful and demonstrate the great potential in magnetic-based SERS assays, they fail to capitalize on the surface enhancement of the magnetic bead. Though the Choo group has attempted coating their microbeads in silver,[12] it has been shown by others such as Park et al.,[13] Carroll et al.,[14] Guven et al.,[15] and Donnelly et al.[16] that using magnetic nanoparticles can significantly improve the SERS enhancement of these assays and, thus, improve the theoretical limit of detection capabilities of this approach.

The magnetic nanoparticle assay presented here utilizes aptamers: high affinity ligands synthesized from short (<100 basepairs) ssDNA folded into a tertiary structure, sensitive to the small toxic molecule BPA.[17,18] These are immobilized onto a combination of plasmonic and magnetic nanoparticles and housed in a convenient magneto-optofluidic chip that can be probed using SERS. Conjugation of the aptamer onto plasmonic nanoparticles labeled with a Raman reporter molecule (RRM), when introduced to a silver-coated magnetic nanoparticle coated in a BPA derivative mediates the formation of nanoparticle assemblies: molecularly bound bundles of stable colloidal nanoparticles which cause a measurable change in the SERS intensity.[19,20] To improve and simplify the detection of the small toxic molecule BPA by its aptamer, multiple plasmonic and magnetic nanoparticle combinations were investigated, and the SERS assay response in both a traditional liquid suspension and housed within a microfluidic chip were analyzed and compared.

2 Experimental Methods

In this paper, the optimization of a "SERS off"[16] competitive binding type assay that utilizes a plasmonic silver (AgNP) and silver-coated magnetic nanoparticle (Ag@MNP) for the detection of the toxin bisphenol A (BPA) is presented (Fig. 1). The assay scheme involves a "target" AgNP functionalized with the Raman reporter dye malachite green isothiocyanate (MGITC) and BPA-binding DNA aptamers bound via a thiolated hexaethylene glycol (HEG) spacer [Fig. 1(b)]. These particles are designed to bind to a version of the toxin bisphenol A diglycidyl ether (BADGE), PEGylated and immobilized onto a second silver-coated magnetic "probe" nanoparticle [Fig. 1(c)], where binding affinities have been determined previously by Marks et al.[18]

When mixed, target and probe nanoparticles cluster into small colloidal networks, creating localized "hot spots" of electric field around the RRMs at the nanoparticle interface, therefore, increasing the polarizability of the Raman reporter, which is observable as an increase in the SERS spectral intensity. This "SERS on" spectral enhancement can then be quantifiably reversed, i.e., "turned-off," by introducing free BPA to the system to compete with the aptamer BADGE interaction, causing the assemblies to release the MGITC-tagged nonmagnetic target AgNPs. Two varietals of ferric nanoparticles, Fe_2O_3 and Fe_2CoO_4, were coated in silver and compared as potential magnetic cores for the probe nanoparticle. The two assays were first characterized in "on" and "off" mode using DLS to verify the formation of nanoparticle network assemblies. Then, the assay was monitored over time by Raman spectroscopy in a standard microwell plate, where assay particles are suspended in solution without magnetic manipulation.

Three different magnetic chip modalities for housing the assay were explored, where particles were housed in microfluidic chips capable of magnetically localizing the assay clusters within a polydimethylsiloxane (PDMS) channel. Raman mapping of the assays' SERS intensity profile when housed within the chips was employed to determine the optimal size of nickel pads patterned within the magnetofluidic channels. Finally, the assay was loaded into a prepackaged, optimized chip and was tested against 2.0 mg/mL of the endocrine disrupting toxin BPA.

2.1 *Materials and Instrumentation*

The modified BPA aptamer,[17] 5'-[ThiSS][HEG]$_3$ CCG CCG TTG GTG TGG TGG GCC TAG GGC CGG CGG CGC ACA GCT GTT ATA GAC GTC TCC AGC-3', was synthesized by Integrated DNA Technologies. Hetero-bifunctional PEG linker (NH_2-PEG-SH, 1 kDa) was purchased from NanoCS. MGITC reporter dye was purchased from Invitrogen (UK). All other reagents were obtained from Sigma Aldrich (USA/UK).

A Varian Cary 300Bio UV–visible spectrophotometer was used with a scan range of 200 to 800 nm for extinction measurements. The zeta potential and hydrodynamic diameters of the nanoparticles were measured on a Zetasizer Nano ZS90 (Malvern, UK). All microplate Raman and SERS spectra were collected using a ThermoScientific DXR Raman confocal microscope with a 900-g/mm grating. SERS mapping of the microfluidic channels was done using a WITec Alpha 300R confocal Raman instrument (WITec GmbH, Ulm, Germany) with a 600-g/mm grating, fitted with a piezodriven XYZ scan stage. All samples were probed using a laser wavelength of 532 nm and coupled to a thermoelectrically cooled charge-coupled device (CCD).

2.2 *Colloid Synthesis*

Silver colloid (AgNP) was synthesized using the "cold" method reported by Leopold and Lendl.[21] Hydroxylamine hydrochloride (1 mL, 150 mM) was added to 89 mL of NaOH (3.33 mM) under vigorous stirring. Silver nitrate ($AgNO_3$) solution (10 mL, 10 mM) was added drop-wise and stirred for 15 min at room temperature. Dynamic light scattering (DLS) measurements revealed an average particle diameter of ~45 nm (not shown) with a PDI index of 0.133. The stock particle concentration was determined to be 225 pM according to Beer's law using an extinction coefficient of 2.87×10^{10} $M^{-1}\,cm^{-1}$ at 404 nm.[22]

Silver-coated cobalt-ferrite nanoparticles ($Ag@Fe_2CoO_4$) were prepared by first synthesizing a stock solution of the core Fe_2CoO_4 nanoparticles through co-precipitation of iron (III) chloride (0.2 M $FeCl_3$) and cobalt(II) chloride (0.1 M $CoCl_2$) in a sodium hydroxide solution at pH ~ 12 (3.0 M NaOH) using a method modified from Donnelly et al.[16] The cobalt ferrite salt solution was added rapidly into 3.5 M NaOH solution under vigorous stirring, then headed at 80°C for 1 h. The cobalt-iron oxide precipitated colloid was washed with deionized water in triplicate using a permanent neodymium magnet. To coat with silver, 500 μL of these stock MNPs was mixed with 4 mL of 0.35 M glucose and 1.5 mL of 60 μM $AgNO_3$. The solution was sonicated for 10 min then heated to 90°C for 90 min. Finally, the particles were centrifuged

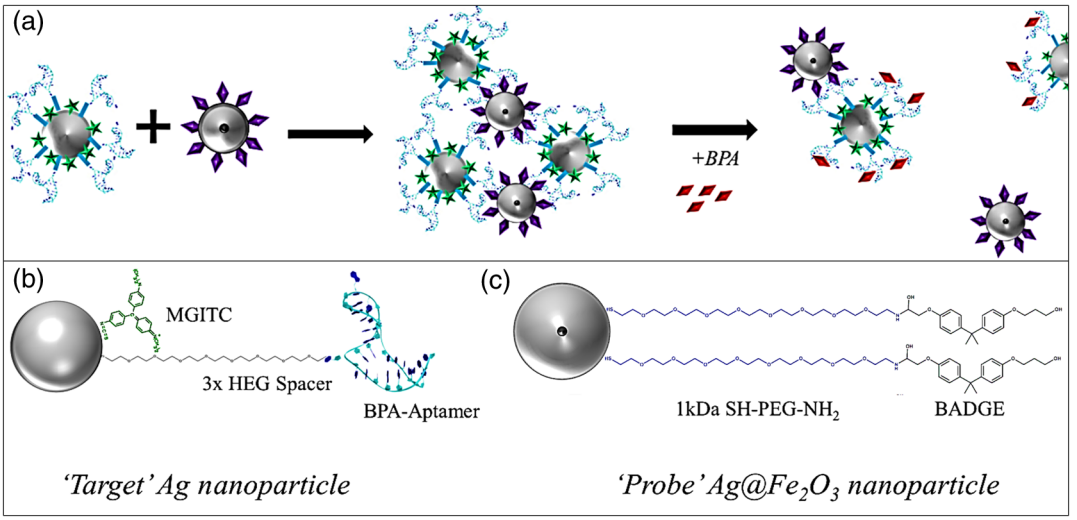

Fig. 1 (a) Schematic illustration of the aptamer mediated "turn-off" SERS competitive binding assay. (b) Target and (c) probe nanoparticle conjugate components.

three times to wash and redispersed in 6 mL of 5 mM sodium citrate.

Silver-coated ferrite nanoparticles ($Ag@Fe_2O_3$) were prepared using a coprecipitation method for the synthesis of the particle core and glucose reduction to coat with silver as described by Kumar et al.[23] and Mandal et al.,[24] respectively. Briefly, a stock solution of maghemite (γ-Fe_2O_3) nanoparticles was prepared by adding 25 mL of an acidified iron salt solution (0.4 M Fe^{2+}, 0.8 M Fe^{3+}, 1 M HCl) drop-wise to 250 mL of 1.5 M NaOH at 50°C under vigorous nonmagnetic stirring. After 20 min, the particles were allowed to cool, washed twice with DI water, and washed once with 0.1 M HNO_3. An additional 125 mL of HNO_3 was then added to the solution, stirred an additional 40 min at 95°C, and resuspended in distilled water. To coat with silver, 1 mL of these stock MNPs was mixed with 4 mL of 0.35 M glucose and 1.5 mL of 60 μM $AgNO_3$. The solution was sonicated for 10 min then heated to 90°C for 90 min. Finally, the particles were centrifuged three times to wash and redispersed in 6 mL of 5 mM sodium citrate.

2.3 *Target and Probe Nanoparticle Conjugation*

2.3.1 *Aptamer/Raman Reporter Molecule AgNP target synthesis*

Prior to immobilization, the BPA aptamers were suspended in a 60-mM phosphate buffer (PBS, pH 8.5) and treated with 15 mg of dithiothreitol (DTT) to reduce their disulfide bonds. After 1 h, the aptamers were purified using a Nanoseps 10 kDa desalting column to remove residual DTT, washing three times in 0.1 M PBS pH 7.4. The aptamers were then heated to 90°C for 5 min to allow any cross-linked DNA to dehybridize, then allowed to cool at room temperature for 15 min to allow sufficient time for the aptamers to fold into their tertiary structure at their strongest folding temperature of $T = 54.1$°C.

Target AgNPs were functionalized with aptamers using a modified method developed by Zhang et al.[25] The aptamer (80 μM) was added to 1 mL of silver colloid (225 pM) at a molar ratio of 2000:1 and left shaking for 1 h. Three 20 μL aliquots of 250 mM citrate HCl buffer (pH 2.9) were then added 5 min apart, and the sample was left an additional 30 min before centrifuging and resuspending the aptamer functionalized particles in 1 mL of 0.3 M PBS (pH 7.4). The RRM, MGITC (10 μM in methanol), was then added at a 500:1 ratio and left to react with the aptamer AgNPs under sonication for 1 h; they were then centrifuged and stored in a 0.1 M PBS buffer (pH 7.4).

2.3.2 *Analyte Ag@MNP probe synthesis*

To synthesize 1 mL of BADGE functionalized magnetic nanoprobes, the SH-PEG-NH_2 linker was added drop-wise to an excess of the analyte BADGE in 0.3 M PBS buffer (pH 8.5) and left overnight to allow conjugation between their terminal amine and epoxide groups respectively. The conjugates were then treated with aminoethanol to open unbound epoxide rings and prevent nonspecific binding of BADGE to the RRM's amine groups. These SH-PEG-BADGE conjugates were then added at a 5000:1 ratio to 1 mL of silver-coated magnetic nanoparticles (stocks diluted to 225 pM). After 1 h, three 20 μL aliquots of 250 mM citrate HCl buffer were again added 5 min apart, and the sample was left an additional 30 min before centrifuging and resuspending the BADGE functionalized particles in 1 mL of 0.1 M PBS (pH 7.4).

2.4 *Analysis of Competitive Binding Assay in a Microwell*

All microwell measurements were collected using the ThermoScientific DXR Raman (600 with a spectral range from 400 to 1800 cm^{-1}) in a total volume of 30 μL) in 0.1 M PBS (pH 7.4) buffer with a 532-nm laser power of 10 mW and an integration time of 10 s (10 × 1 s exposures). A solution containing equal volumes of 225 pM of each of the target and probe nanoparticles was monitored with SERS for 5 h to allow complete binding between the immobilized BPA aptamers and BADGE. The assembled nanoparticle clusters were collected using a neodymium magnet held at the side of the glass vial, the supernatant containing any unbound AgNPs was removed, and the assembled nanoparticles were resuspended in 0.1 M PBS (pH 7.4). For confirmation of the formation of nanoclusters using DLS, 10 μL of the assembled target/probe NPs were mixed and allowed to shake for 3 h before collecting size measurements. To monitor competitive binding with SERS, 20 μL of

the assay clusters were mixed with 10 μL of BPA (1 pM to 1 μM) in 0.1 M PBS (pH 7.4), and SERS measurements were taken every 30 s for 6 min.

2.5 *Fabrication of Ni-Patterned Magnetic Microchannel*

Each magnetofluidic SERS chip is composed of a 200-nm-thick deposited nickel patterned onto a glass microscope slide, a PDMS microfluidic channel, and two permanent neodymium magnets housed around the PDMS chip by a 3-D printed casing. COMSOL was used to simulate the distribution of induced magnetic field for different designs by mapping the theoretical magnetic flux density for the experiment and are shown in Fig. 2. From modeling, it was revealed that at least two pads are necessary to evenly distribute the magnetic field in the channel, which would lie perpendicular to the gap line in the red zone of 2(a). Figure 2 shows the initial two designs investigated: design A "the straight pattern" [Figs. 2(a) and 2(c)] and design B "the micromagnet array" pattern [Figs. 2(b) and 2(d)]. The magnetic field across the patterns (where the PDMS channel will be overlaid) is induced by the two attractive permanent neodymium magnets on either side of the pads, as shown in the schematics in Figs. 2(c) and 2(d). In these schematics, the polarity for the top magnet is north and for the bottom magnet is south; therefore, the polarity of the induced field across the pattern is reverse (top of the pattern is the south pole and bottom is north pole). This is due to the induced magnetic field propagating down the deposited nickel from the field, looping from the top to the bottom external magnets. From the magnetic flux density maps in Figs. 2(a) and 2(b), it is observed that the field is strongest at the centers and edges of the nickel pads for both patterns; thus, it is predicted that the majority of magnetic nanoparticles will be trapped at the "warm" locations within the

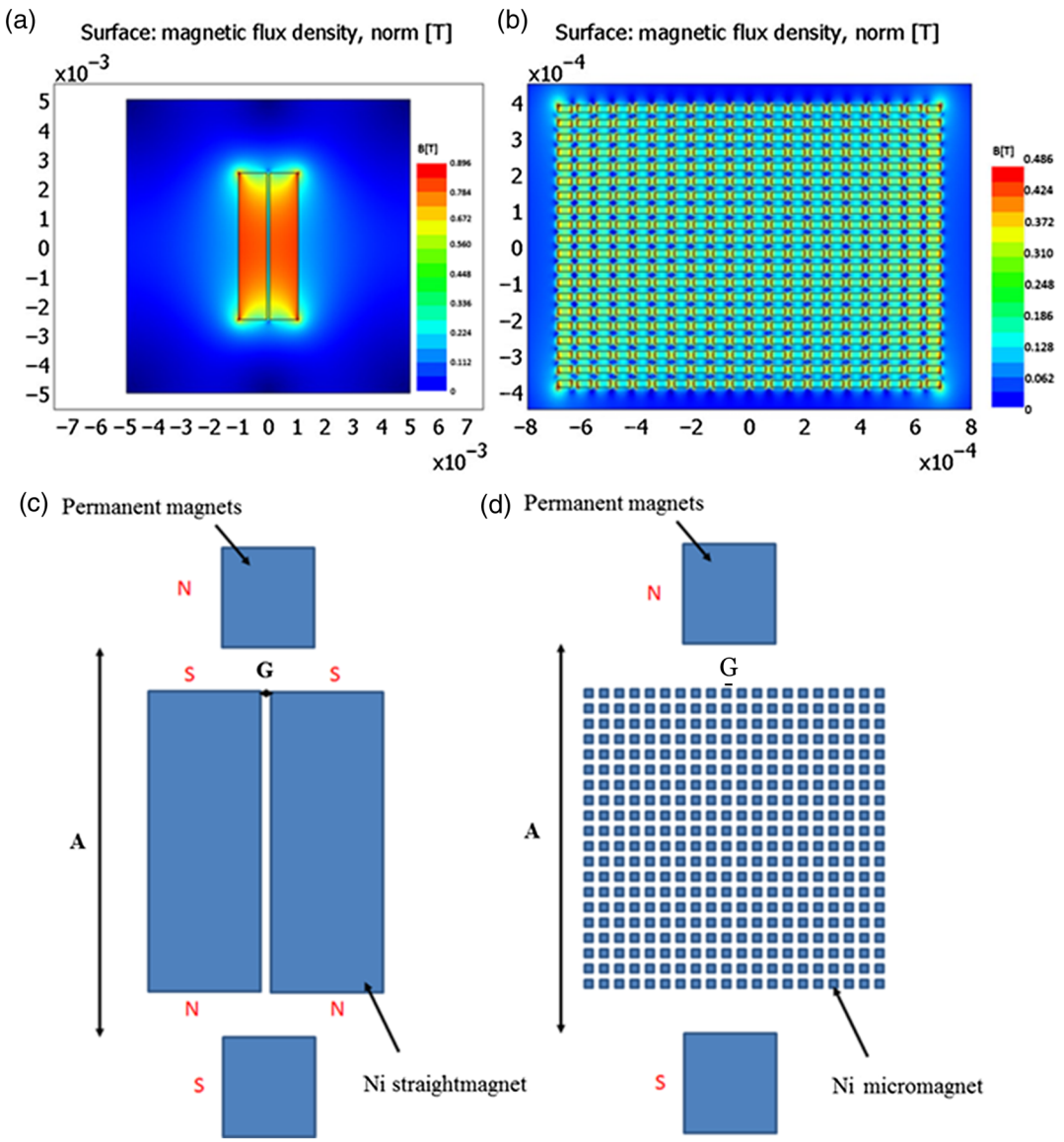

Fig. 2 COMSOL simulation results of the magnetic flux density intensity distribution for (a) straight Ni-pads and (b) an array of Ni-pads, demonstrating that the magnetic field is stronger for a planar field of Ni but is more evenly distributed for the array pattern. It is desired that the magnetic field is uniform but not too strong as to aggregate the particles irreversibly on the surface of the nickel. Schematic diagram for (c) straight and (d) array micromagnet design patterns. $A = 1$ cm, $G = 50$ μm

patterns where the magnetic flux density is the strongest. Since each micropad has its own distribution of magnetic flux density, each micropad can be considered as an individual micromagnet, thereby creating a series of "magnetic microwells" when housed in a fluidic chip. It is noted that it is desirable that the magnetic field is not too strong as to aggregate the particles irreversibly on the surface of the nickel. A weaker field also allows space for competitive binding to cause the release of a nonmagnetic nanoparticle without it being captured by another magnetic probe downstream. According to Do et al.,[26,27] the magnetic field distributed to Ni-pads with nanaometer-thickness should distribute vertically with a height of ~20 μm.

To fabricate the chips, the nickel is deposited onto a glass microscope slide by photolithography and electron beam deposition using a methodology derived from Guven et al.[15] Briefly, glass slides are spin-coated with lift-off resist (LOR) 3A and S-1813 LOR at 750 nm and 1.3 μm, respectively. After exposure and development, the pattern of the Ni micromagnet array is visibly transferred onto the glass slides. Next, 100-nm-thick chromium and 50-nm-thick copper are continuously deposited on the pattern as the adhesion layer, and then 200-nm-thick nickel is deposited as the third and final "magnetically responsive layer." After deposition, the entire glass slide is placed into the chemical stripper of LOR 3A at 80°C to remove the photoresist layer. A 100-μm-thick microfluidic channel is constructed using a silicon wafer mold via soft lithography. Uncured-PDMS solution (10:1) is poured over the silicon wafer mold and cured at 65°C for 2 h as per typical soft lithography methods.[16] Finally, the PDMS microfluidic channel is bound to the glass slide patterned with a micromagnet array by plasma etching treatment. The nickel pads within the channel are not magnetically activated until the final 3-D printed neodymium magnet holder is placed around the channel.

2.6 *SERS Analysis of Prebound Assay Particles Housed in Magnetofluidic Chip*

A 200-μL solution containing equal volumes of 225 pM of each of the target and probe nanoparticles in a total volume of 300 μL 0.1 M PBS was allowed to flow through the Ni-patterned magnetic channels at a 2 mL syringe pump rate of 10 μL/min, and subsequentially left overnight to dry. After reintroducing particles to 0.1 M PBS, the SERS profile of the localized assembled nanoparticle clusters were mapped using WiTec Raman analysis software for chip designs A & B and using Thermo-Scientific DXR Raman Omnic mapping software for chip design C. Both the WiTec and Thermo-Scientific Raman microscopes use a 10× objective (NA 0.25), 600 lines/mm grating, and a 10-mW 532 nm laser, where all SERS measurements were collected with an integration time of 2 s (2 × 1 s total exposure) and a step size of 10 μm. Seventeen maps were collected for a total 3-D mapping area of $3 \times 300 \times 170$ μm (XYZ) for chip design A. Additionally, 2-D maps were scanned for areas of 75 μm × 75 μm (XY) for design B and 70 μm × 350 μm (XY) and 70 μm × 70 μm (XZ) for chip design C. Raman spectral maps of the MGITC peak at 1175 cm^{-1} were processed using Origin Pro 2015 graphing software.

3 Results and Discussion

3.1 *Target and Probe Nanoparticle Conjugation*

As shown from the SEM images and DLS plots in Fig. 3, the average hydrodynamic particle diameter of probe 1 ($Ag@Fe_2O_3$, nanoparticles coated in BADGE) was determined by DLS to be ~70 nm, with a final concentration of 425 pM as determined by a Nanosight NTA. For probe 2, the iron core was doped with cobalt to increase the magnetization of the probe particles and improve the collection time. Probe 2 $Ag@Fe_2CoO_4$ particles were ~63 nm in diameter, and final stock concentration was 385 pM as determined by NTA. The extinction profile of plain AgNPs compared to the magnetic core–shell particles ($Ag@Fe_2CoO_4$ and $Ag@Fe_2O_3$) is shown in Fig. 3(c) for reference.

A colloid's zeta potential (ζ) is indicative of the relationship between the particles' surface charge and their ionic environment and thus can be used to predict long-term stability. The Ag target nanoparticles were functionalized with aptamers and MGITC as described and yielded an average ζ of −39.7 mV, where $\zeta > -20$ mV indicates sufficient colloidal stability. Silver-coated probe particles of the Fe_2O_3 and Fe_2CoO_4 varietals-coated in PEGylated BADGE were found to have zeta potentials of −32.1 and −22.7 mV, respectively (Fig. 3), indicating that the PEG spacer and the HEG modified aptamer provide adequate particle stabilization in the 0.1 M PBS binding buffer but that the Co-doped particles were slightly less stable.

3.2 *Analysis of Competitive Binding Assay in a Microwell*

The SERS response of the probe and target nanoparticles as they form assembled assay nanoclusters, along with the nanocluster assay's subsequent negative SERS response when introduced to competing BPA, was first analyzed in a traditional microwell-plate. As shown in Fig. 4(a), the SERS signal of the reporter molecule MGITC exhibits a 50-fold increase in SERS intensity as it experiences an increase in the electron density in its immediate environment due to the aptamer-induced plasmonic nanoparticle assembly, reaching a steady-state equilibrium after ~2 h. The DLS results in Fig. 4(b) show that upon probe and target binding, the average size of the colloid increases, which can be interpreted as formation of the assay nanoclusters. Bringing the nanoparticles closer together as the DLS indicates increases the net field intensity as hot spots form, which leads to the increase SERS intensity.

When free BPA is added to the assay nanoparticle assembly solution, it competes with BADGE on the surface of the probe particle for the aptamer binding sites on the target particle (Fig. 5). This dissociation is verified by the decrease in SERS intensity of the peak at 1175 cm^{-1} [aromatic C–H bending vibrational mode,[28] Fig. 5(a)] and decreases to a steady state over the course of ~5 min as competitive binding occurs [Fig. 5(b)]. This implies that the BPA aptamer immobilized on the target AgNPs must "loosen" (increased net interparticle distance) or release from the BADGE on the MNPs to more favorably bind to free BPA. This causes a decrease in the solution SERS signal due to MGITC being displaced further from the nanoparticle surface interface *quantifiably* as hypothesized and as demonstrated in Fig. 5(c).

3.3 *SERS Analysis of Prebound Assay Particles Housed in Magnetofluidic*

To develop a more repeatable SERS analysis platform for assays relying on magnetic nanoparticles, PDMS microchannels laid over two Ni-Patterned glass slides that can be magnetically activated by two neodymium magnetic encased around the

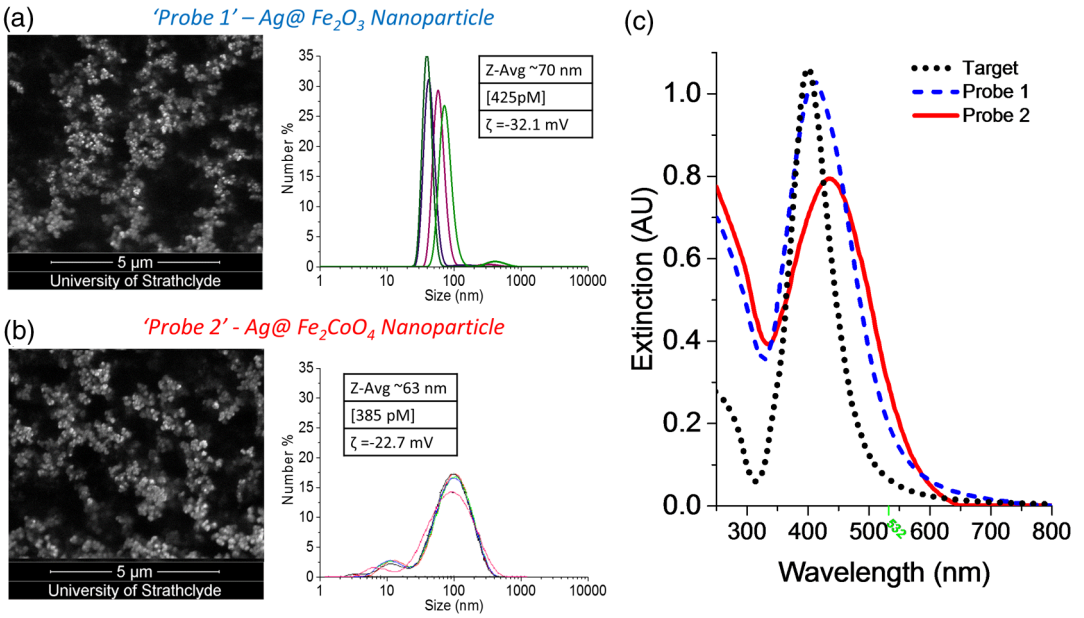

Fig. 3 (a) SEM images of the two ferric probe nanoparticles after coating in silver to enhance their plasmonic properties at 532 nm, (b) DLS size distribution, concentration, and zeta potential data demonstrating particle size, yield, and stability, and (c) comparison of the extinction profile of the target solid silver target nanoparticles (black dots) with the two silver coated Fe (blue dash) and FeCo (red line) probe nanoparticles.

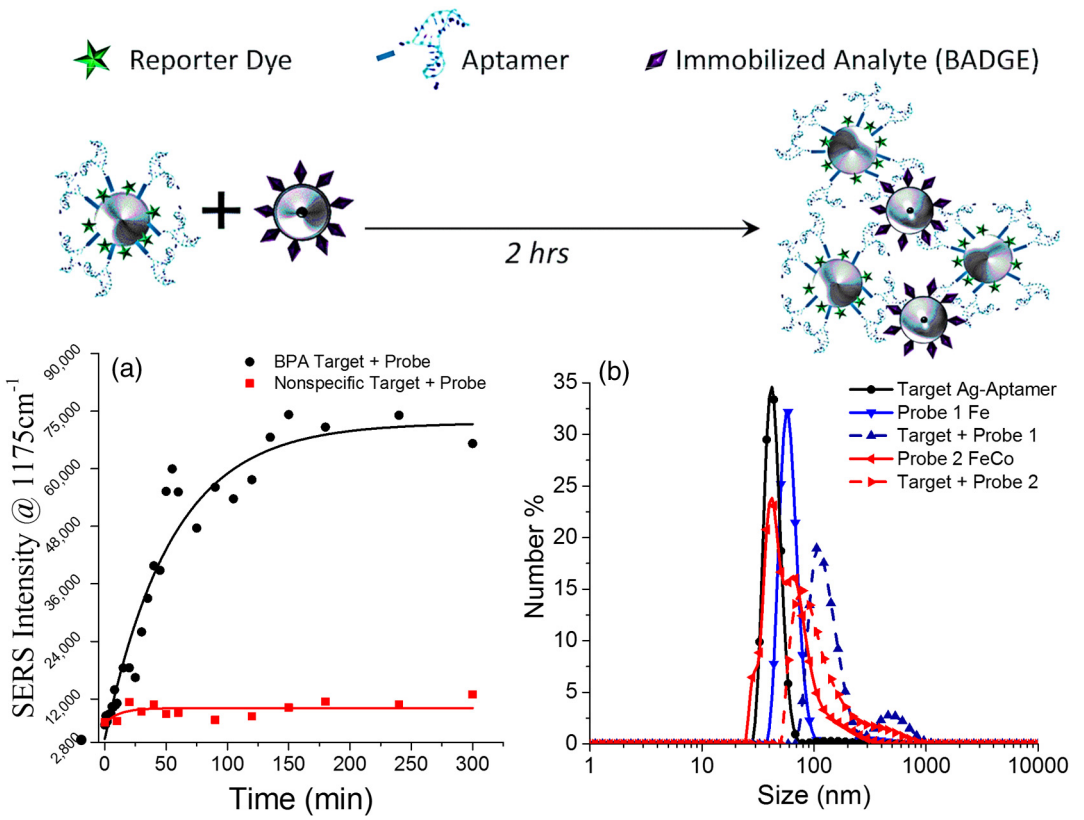

Fig. 4 Schematic of nanocluster assembly (a) SERS spectral intensity from tagged target nanoparticle, conjugated to either a BPA specific (black circle) or a nonspecific (red square) aptamer sequence, monitored for 5 h after exposure to the Ag@Fe probe nanoparticles at a 1 : 1 molar ratio. Correlation coefficient of the exponential fit of the stagnant nanoparticle assembly is $r^2 = 0.94$ and reaches equilibrium after ~2 h. (b)Verification by DLS that SERS enhancement is facilitated by nanoparticle assemblies, shown before and after for each probe type.

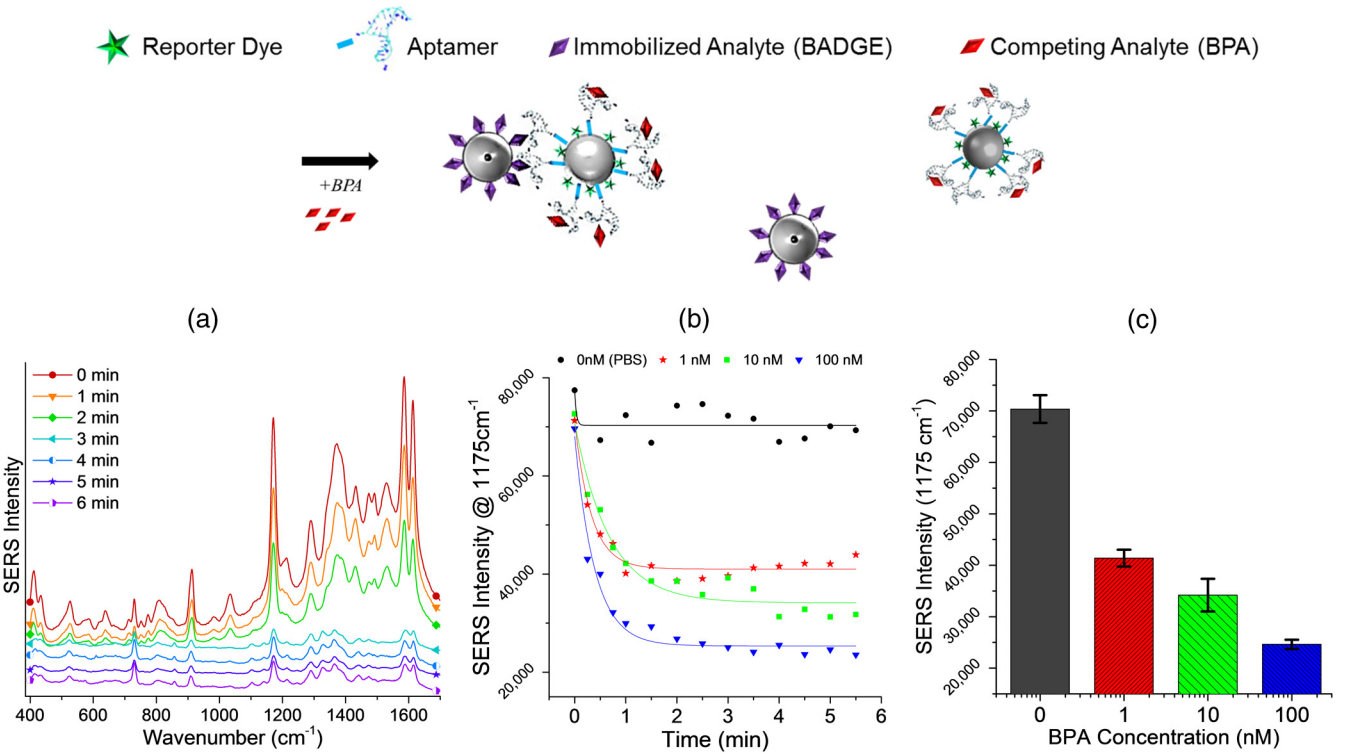

Fig. 5 Schematic of nanocluster dissociation in the presence of the analyte BPA. (a) SERS spectra of assay nanoclusters taken at 1 min intervals for 6 min after exposure to 10 nM BPA. (b) Nanocluster assay response after exposure to 0 to 100 nM of the competing analyte BPA in free solution as a function of time, where the r^2 coefficient of the fits for the time response curves against 1, 10, and 100 nM BPA were 0.96, 0.95, 0.97, respectively. (c) Average SERS peak intensity at 1175 cm^{-1} after 5 min of reaction time with BPA as a function of concentration.

optofluidic chip were developed (Fig. 6). Specifically, the magnetic collection rate and the SERS enhancement of silver-coated Fe_2O_3 and Fe_2CoO_4 nanoparticles bound to the Ag target particles were compared for two different Ni-pattern designs as shown in Fig. 6: straight (chip design A—center images) and spotted (chip design B—right images).

Using 3-D Raman mapping, the straight channel (chip A) provided a more uniform nanoparticle organization with an apparent coefficient of variation of 23.6% across the entire channel when in focus with the Ni pads. However, only the assay with the less stable Co-doped $Ag@Fe_2CoO_4$ probe was magnetically trapped within chip design A. This was likely due to its rapid magnetic collection rate (on the order of minutes compared to hours required to pull down 2 mL in a glass scintillation vial) when compared to the "plain" but stable ferric particles. To investigate, a depth profile of the straight channel after exposure to 200 μL of Co-doped ferric assay nanoparticle clusters was obtained in the form of 3-D Raman spectroscopic maps (Fig. 7).

The map in Fig. 7 reveals that the large majority of particles are located at the bottom of the channel, near the surface of the deposited nickel. Unfortunately, exposure to BPA competing analyte as high as 2 mg/mL (an order of magnitude above the physiological range) revealed no statistically relevant change in the SERS intensity in the channel. It is hypothesized that this is due to the magnetic field delivered to the pads being too strong at its surface and not reaching the full height of the channel with uniformity. This forces the particles too close together, hindering competitive binding or even causing irreversible mechanical aggregation. This is consistent with the COMSOL models in Fig. 2, which predict that the magnetic field is much stronger for a planar field of Ni when compared to an array pattern. Additional error in the particle depth distribution could be due to the fact that only the polydisperse, unstable $Ag@Fe_2CoO_4$ probe assay was trapped within chip design A. While this design was simpler to pattern, and the Fe_2CoO_4 core being the much simpler choice in terms of synthesis, it was determined that this "quick and easy" modality is not sufficient for monitoring molecular binding events with SERS. However, it may still be valuable as a simple solution for controlling magnetic nano (or micro) particles for assay wash steps. This design could be used to either automate washing steps and buffer exchanges or automate the capture and enhancement of the spectra of specific components in a complex solution.

Chip design B, consisting of a 2×5 Ni-pad array, was able to trap the more stable $Ag@Fe_2O_3$-based assay. Chip B demonstrated a 10-fold improvement in the localized SERS enhancement (Fig. 8) across the nickel pads when compared to chip A and, thus, theoretically allows for lower limits of detection. Since the COMSOL models in Fig. 2 revealed that the magnetic field would be weaker but more evenly distributed for the array pattern, we suspect that the increase in SERS enhancement is due to an increase in the number of assay particles trapped not an increase in the magnetic field strength. In terms of quantification limits, looking at the raw peak intensity at 1175 cm^{-1} the coefficient of variation (%CV) across all 10 pads was at nearly 55%, though intensity maps in Fig. 8 reveal this is mainly due to a larger portion of particles located on the top row of pads. This is likely due to several incomplete nickel pads in

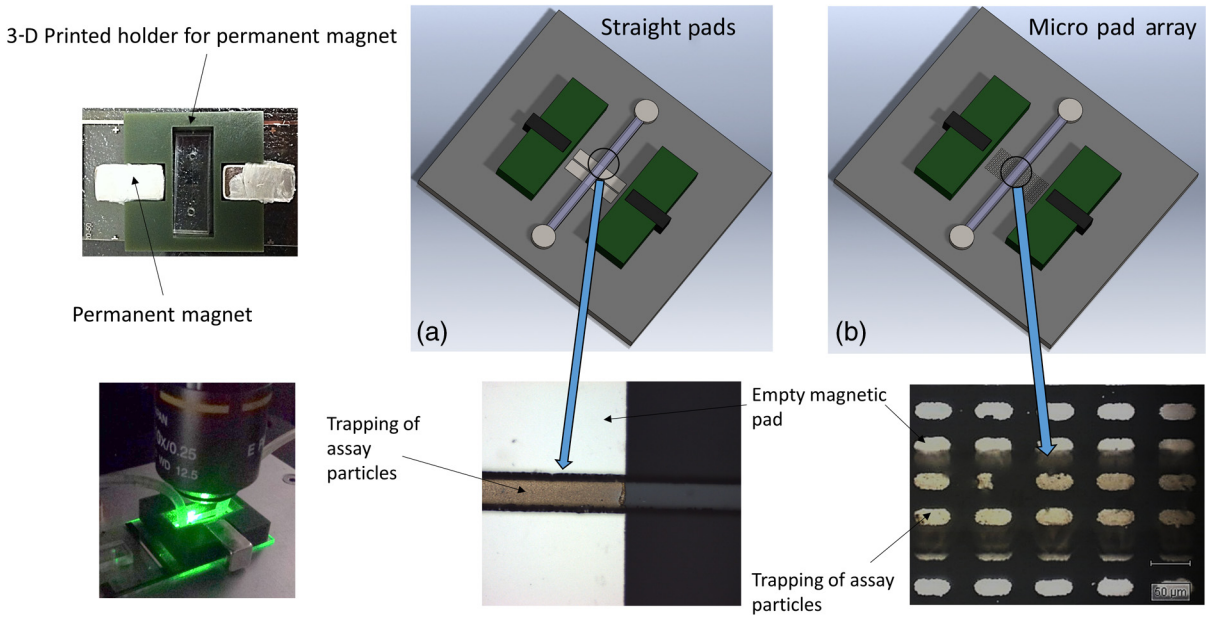

Fig. 6 Magnetofluidic chip designs: (a) Top-down and isometric images of the experimental setup for Raman mapping of the assay nanoparticle clusters within the magnetic microfluidic. (b) Schematic and brightfield images of the Ni-patterned detection regions through a 10× objective for chip design A. (c) Same as center for chip design B.

the bottom row, which prevent the magnetic field from propagating uniformly across the pads. Unfortunately, depth profiles for design B were unable to be obtained as the small pad's field was still too concentrated near the surface, yielding-enhanced assay signal only when in focus with the nickel pad as before.

To overcome the issues with chip designs A and B, a more optimized chip C nickel pad pattern was designed. Chip design C involves a 1×5 array of magnetically activated pads housed within the PDMS channel (Fig. 9, left), which provides similar benefits as Chip B while avoiding the error induced by having two full rows of pads within the channel. This design allows the field to propagate in a manner that provides individual pad fields strong enough to trap the weakly magnetic yet stable $Ag@Fe_2O_3$-based assay while also providing uniform SERS enhancement in the Z-dimension. In other words, it is desired that the colloid is suspended in solution in the channel and that particles are not irreversibly aggregated by the field pulling them too close together or onto the nickel surface so that they may avoid steric hindrance when exposed to BPA.

Top-down Raman intensity maps of chip loaded with the Fe_2O_3-based assay design C are also shown in Fig. 9. When the channel is filled with dried assay particles, the chip

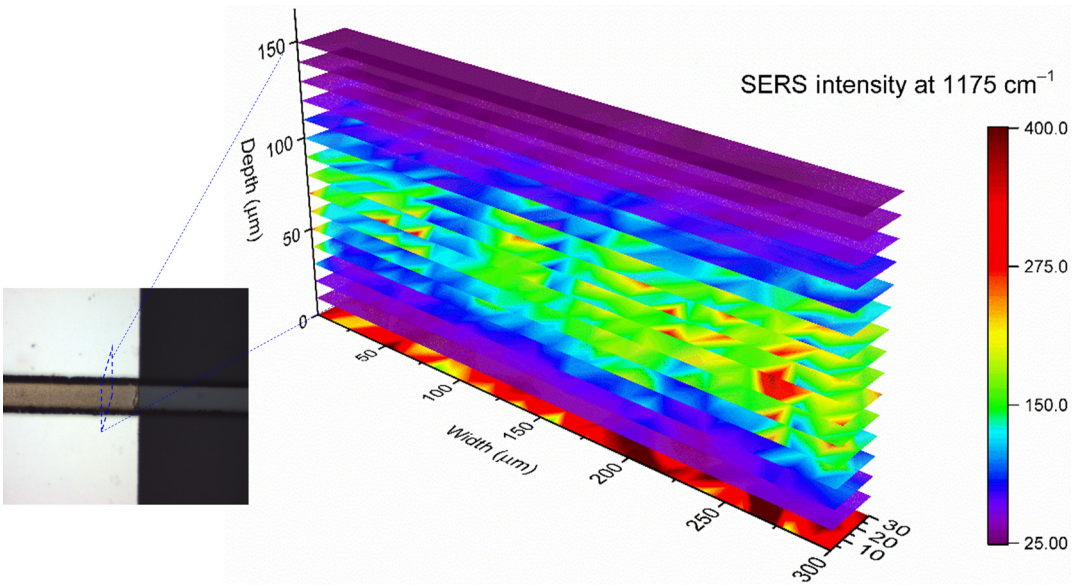

Fig. 7 Chip design A 3-D intensity profile: 17-stacked XY Raman intensity maps of the straight channel design filled with Ag@FeCo assay clusters, revealing that the majority of particles are located at the bottom of the channel near the surface of the nickel pad.

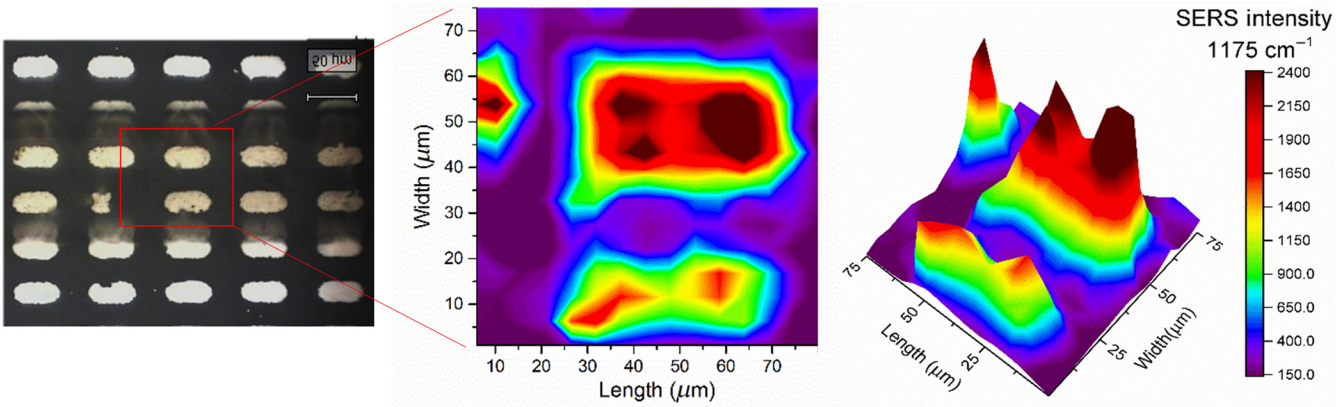

Fig. 8 Chip design B Raman *XY* intensity profile: looking at the center column from the 2×5 array of Ni pads it is noticeable that particles favor the top row of pads, which are more uniform than the bottom row and thus provide a more uniform field.

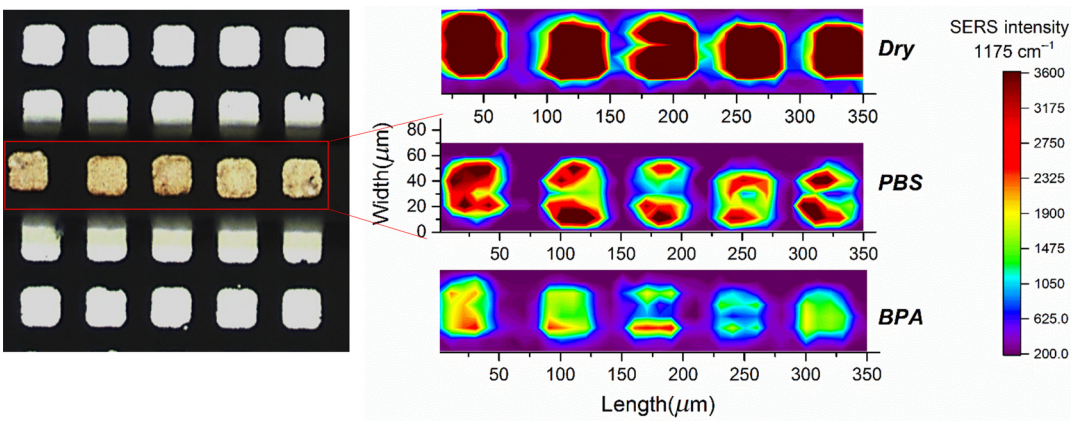

Fig. 9 Chip design C Raman *XY* intensity profile and response to BPA: looking at the entire length of the 1×5 array of Ni pads. It is noticeable that SERS intensity of the particles is redistributed when buffer is introduced, indicating particle resuspension. Upon introduction of 2 mg/mL of BPA, the net SERS intensity over each pad decreased in response to competitive binding.

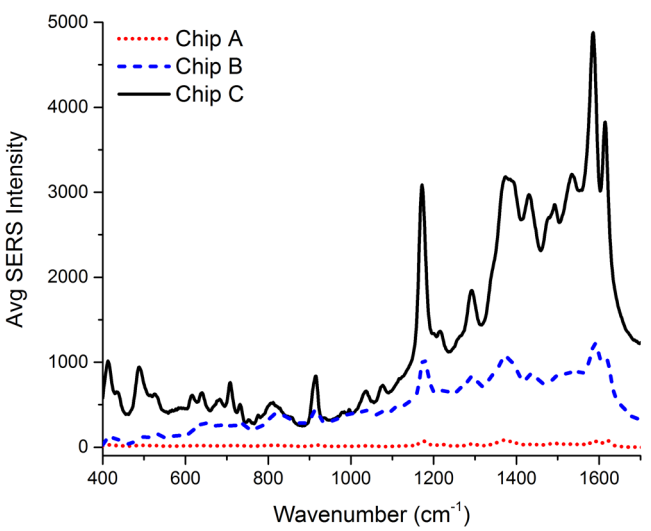

Fig. 10 SERS spectra for the average across the entire Ni patterned area for all three chip designs. Here, it is observed that chip C provides a 30-fold enhancement compared to chip A, and a 3-fold enhancement compared to chip B.

demonstrated SERS enhancements up to 5 times higher than design B and 30 times higher than design A, as demonstrated by comparing their averaged full spectra over the nickel patterns in Fig. 10. However, for a more clear comparison across all three conditions, the map of the dried assay in Fig. 9 is scaled to the maximum intensity of the PBS chip, which was 1.5 times higher than chip B and 9 times higher than chip A. The PBS filled channel, where the map was collected 10 μm above the pad surface, provides ample space for particle suspension and verifies that after filling the dried assay in the channel with PBS the particles are redispersed. This is further confirmed by an overall drop in the SERS intensity, which remained steady over 1 h after the full 300 μL of particles passed through the chip. Additionally, upon introduction of 2 mg/mL of BPA, a drastic drop in the SERS intensity at 1175 cm^{-1} was observed after 5 min, consistent with the behavior seen when testing the assay in the well plate and thus validating the chips capability for housing a molecularly mediated SERS assay.

To confirm that particles were not permanently bound to the nickel pads, depth profiles (*XZ*) of chip design C were collected with and without the syringe pump turned on at 10 μL/min (Fig. 11). When the pump is on, the particles' signal moves with the direction of flow. Although the %CV across the entire

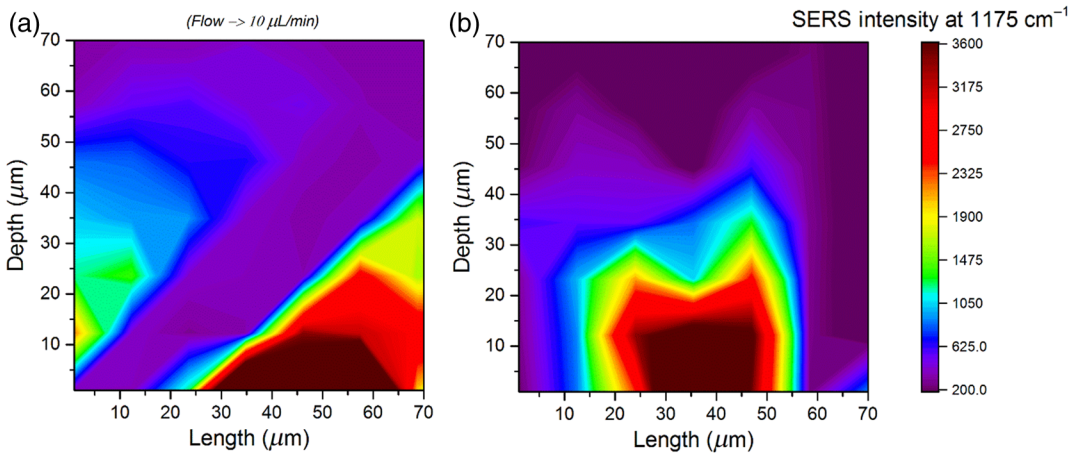

Fig. 11 Chip design C Raman intensity depth profile: looking at the depth profile of the second pad in the array. (a) Map shows that assay clusters are not bound to the surface and are able to move with the pump flow as a colloidal suspension. (b) Map shows assay cluster reorganize over the center of the pad when the pump is turned off.

channel for design C is still ~50% as with design B, while investigating the signal variability across each individual pad it was discovered that the error could be reduced through individual normalization to the each of the five pads' maximum intensity at time $t = 0$ (i.e., when the channel is filled with PBS). The improved standard error of the mean of the five chips yielded a %CV of ~25%, further improving upon the previous designs.

4 Conclusion

A "turn-off" SERS assay platform methodology has been described for the detection of small toxins utilizing aptamer-mediated assembly of colloidal nanoparticles into nanoclusters. This colloidal SERS assay is formed through the mixing of probe (antigen) and target (aptamer-dye) nanoparticles and reaches an equilibrium after ~2 h. A 3 to 5-min competitive binding event initiated by the presence of as little as 10 μL of 1 nM bisphenol A in free solution was monitored. It was determined that the probe nanoparticles have specific preference for the BPA aptamer target particles, and the particles competitively bind with free BPA as well, implying that no nonspecific binding occurred. This approach has the potential to be translated to any aptamer/antigen pair and provides the added benefit of magnetic manipulation of the nanoparticle sensing network to remove any unbound nanoparticles that could potentially interfere with the Raman readout.

Three magnetic microfluidic chip modalities were designed and tested with the two magnetic probe NP core types. It was found that the Ag@Fe_2O_3 particles were, on average, larger yet more uniform in size and more stable than Ag@Fe_2CoO_4. However, the addition of cobalt significantly improved the collection time of particles within the magnetic chips and was also a much simpler synthesis method for the ferric core. Using 3-D Raman mapping, the straight channel (chip A) design with the Ag@Fe_2O_3 particles intrinsically provided the most uniform nanoparticle organization; however, particles were found to be localized mostly directly on the surface of the pad. While not suited for this application, this design is the simplest to produce and could prove valuable for rapid prototyping of other magnetic nanoparticle assays.

While the nickel pad array channel chip design B was able to capture the desirable Ag@Fe_2O_3 particles and demonstrated a larger SERS enhancement, and thus a lower overall limit of detection, it had extreme variability between its 10 pads. For the chip C design, using larger 50 μm × 50 μm square pads, it was found that the pad to pad variability could be reduced to 25% through normalization to the maximum intensity within a pad. Additionally, it was demonstrated that this uniform signal could be obtained as far as 20 μm from the surface of the nickel pads and was able to demonstrate the desired "SERS off" assay-competitive binding response to BPA. Therefore, the chip C design used in conjunction with the Fe_2O_3 magnetic core varietal of the probe nanoparticle was the most successful iteration of the experiment for monitoring BPA. Due to the intrinsic properties of colloidal plasmonic nanoparticles, this platform technology could potentially be tuned to virtually any biomarker-sensing ligand pair and even multiplexed using multiple RRMs.

Disclosures

There are no competing interests.

Acknowledgments

H.M., P.J.H., J.K., and G.C. wish to acknowledge the financial support from the National Institute of Environmental Health Sciences of the National Institutes of Health under Grant Nos. 2R44ES022303 and P30ES023512. The content is solely the responsibility of the authors and does not necessarily represent the official views of the National Institutes of Health. S.M. and D.G. acknowledge support from the EPSRC Engineering and Physical Sciences Research Council (EP/L014165/1). H.M. also wishes to acknowledge the Whitaker International Foundation for its fellowship support that facilitated this collaborative work. H.M. would like to thank Steven Asiala and Alexandre Girard of the University of Strathclyde, Mitchell Robinson of Texas A&M University, Mariana Diaz of Universidad Autónoma de Yucatán, and Bill Jackson at Base Pair Biotechnologies (Pearland, Texas) for their assistance and helpful technical discussions on the use of aptamers and Raman mapping and data processing. As per SPIE guidelines, the authors acknowledge the SPIE Photonics West proceedings number 9722-0N, in which part of this work was presented in San Francisco, California, on February 14, 2016. As per SPIE

guidelines the authors acknowledge that a portion of this work was included in SPIE BIOS conference proceedings number 9722-0N, which was presented at the Photonics West meeting in San Francisco, CA on Feb. 14, 2016.

References

1. F. Collins, "Has the revolution arrived?," *Nature* **464**, 674–675 (2010).
2. L. Hood et al., "Systems biology and new technologies enable predictive and preventative medicine," *Science* **306**, 640–643 (2004).
3. S. M. Rappaport, "Implications of the exposome for exposure science," *J. Exposure Sci. Environ. Epidemiol.* **21**, 5–9 (2011).
4. C. M. Rocheleau et al., "Maternal exposure to polychlorinated biphenyls and the secondary sex ratio: an occupational cohort study," *Environ. Health* **10**, 20 (2011).
5. M. Gellner, K. Kompe, and S. Schlucker, "Multiplexing with SERS labels using mixed SAMs of Raman reporter molecules," *Anal. Bioanal. Chem.* **394**, 1839–1844 (2009).
6. S.-Y. Chen and A. A. Lazarides, "Quantitative amplification of Cy5 SERS in 'warm spots' created by plasmonic coupling in nanoparticle assemblies of controlled structure," *J. Phys. Chem. C* **113**, 12167–12175 (2009).
7. M. Gellner et al., "SERS microscopy: plasmonic nanoparticle probes and biomedical applications," *Proc. SPIE* **7757**, 77570M (2010).
8. Ž. Krpetić et al., "Importance of nanoparticle size in colorimetric and SERS-based multimodal trace detection of Ni(II) ions with functional gold nanoparticles," *Small* **8**, 707–714 (2012).
9. J. Yoon et al., "Highly sensitive detection of thrombin using SERS-based magnetic aptasensors," *Biosens. Bioelectron.* **47**, 62–67 (2013).
10. R. Gao et al., "Fast and sensitive detection of an anthrax biomarker using SERS-based solenoid microfluidic sensor," *Biosens. Bioelectron.* **72**, 230–236 (2015).
11. H. Chon et al., "On-chip immunoassay using surface-enhanced Raman scattering of hollow gold nanospheres," *Anal. Chem.* **82**, 5290–5295 (2010).
12. B. Han et al., "Application of silver-coated magnetic microspheres to a SERS-based optofluidic sensor," *J. Phys. Chem. C* **115**, 6290–6296 (2011).
13. H. Y. Park et al., "Fabrication of magnetic core @ shell Fe oxide @ Au nanoparticles for interfacial bioactivity and bio-separation," *Langmuir* **23**, 9050–9056 (2007).
14. K. J. Carroll et al., "Surface enhanced Raman utilizing magnetic core gold shell nanoparticles," in *Nanotechnology 2010: Advanced Materials, CNTs, Particles, Films and Composites–Technical Proc. of the 2010 NSTI Nanotechnology Conf. and Expo, Nsti-Nanotech 2010*, **1**, 395–398 (2010).
15. B. Guven et al., "SERS-based sandwich immunoassay using antibody coated magnetic nanoparticles for Escherichia coli enumeration," *Analyst* **136**, 740–748 (2011).
16. T. Donnelly et al., "Silver and magnetic nanoparticles for sensitive DNA detection by SERS," *Chem. Commun.* **50**(85), 12907–12910 (2014).
17. M. Jo et al., "Development of single-stranded DNA aptamers for specific bisphenol a detection," *Oligonucleotides* **21**, 85–91 (2011).
18. H. L. Marks et al., "Rational design of a bisphenol a aptamer selective surface-enhanced Raman scattering nanoprobe," *Anal. Chem.* **86**, 11614–11619 (2014).
19. H. Marks et al., "Comparison of Fe_2O_3 and Fe_2CoO_4 core-shell plasmonic nanoparticles for aptamer mediated SERS assays," *Proc. SPIE* **9722**, 97220N (2016).
20. H. Marks et al., "SERS active colloidal nanoparticles for the detection of small blood biomarkers using aptamers," *Proc. SPIE* **9338**, 93381C (2015).
21. N. Leopold and B. Lendl, "A new method for fast preparation of highly surface-enhanced Raman scattering (SERS) active silver colloids at room temperature by reduction of silver nitrate with hydroxylamine hydrochloride," *J. Phys. Chem. B* **107**, 5723–5727 (2003).
22. J. Yguerabide and E. E. Yguerabide, "Light-scattering submicroscopic particles as highly fluorescent analogs and their use as tracer labels in clinical and biological applications: I. Theory," *Anal. Biochem.* **262**, 137–156 (1998).
23. G. Kumar et al., "Metal-coated magnetic nanoparticles for surface enhanced Raman scattering studies," *Bull. Mater. Sci.* **34**, 207–216 (2011).
24. M. Mandal et al., "Magnetite nanoparticles with tunable gold or silver shell," *J. Colloid Interface Sci.* **286**, 187–194 (2005).
25. X. Zhang et al., "Fast pH-assisted functionalization of silver nanoparticles with monothiolated DNA," *Chem. Commun.* **48**, 10114–10116 (2012).
26. J. Do and C. H. Ahn, "A polymer lab-on-a-chip for magnetic immunoassay with on-chip sampling and detection capabilities," *Lab Chip* **8**, 542–549 (2008).
27. J. Do, J. W. Choi, and C. H. Ahn, "Low-cost magnetic interdigitated array on a plastic wafer," *IEEE Trans. Magn.* **40**, 3009–3011 (2004).
28. A. C. Power, A. J. Betts, and J. F. Cassidy, "Non aggregated colloidal silver nanoparticles for surface enhanced resonance Raman spectroscopy," *Analyst* **136**, 2794–2801 (2011).

Haley Marks is currently a doctoral candidate in biomedical engineering at Texas A&M University under Dr. Gerard Coté. She received her BS degree from Boston University in 2011, was a 2014 Whitaker International Fellow, and a 2016 Ocean Optics Young Investigator award recipient. Her current research interests include translational biophotonics, nanotechnology, point-of-care diagnostics, and bioanalytical sensors. She is an active member of SPIE and was the Texas A&M SPIE student chapter president in 2015.

Po-Jung Huang is pursuing his PhD in the Department of Material Science and Engineering at Texas A&M University. His research focus is on the development of microfluidic devices for single molecular detection, especially protein complexes and biotoxins. He also concentrates on manufacturing cell and bacteria microenvironment via hydrogel for cancer research and waste water treatment. He is a current member of SPIE.

Samuel Mabbott is currently a postdoctoral research assistant in the Nanometrology group at the University of Strathclyde. He completed his PhD in biochemistry at the University of Manchester in 2012 and MChem at the University of Sheffield in 2008. His interests include the strategic design of nanoparticles for diagnostic assays and the application of nanoparticles to photothermal therapy.

Duncan Graham is a research professor of chemistry and head of Department for Pure and Applied Chemistry at the University of Strathclyde in Glasgow. He completed a PhD in organic chemistry at the University of Edinburgh in 1996 and his interests are in developing new diagnostic assays based on nanoparticles and spectroscopy with target molecules including DNA, RNA, proteins and small molecule biomarkers.

Jun Kameoka is an associate professor in the Department of Electrical and Computer Engineering, Material Science and Engineering at Texas A&M University. He is also affiliated as an adjunct professor with the Frontier Medical Engineering Department at Chiba University and Tokyo Jikei School of Medicine in Japan. His expertise is nano and microfluidics, micro- and nanosensors, and actuators. He has been awarded 10 U.S. and Japanese patents and published over 100 journal articles and conference proceedings.

Gerard Coté is the director of the Center for Remote Health Technologies and Systems and holder of the Charles H. & Bettye Barclay professorship within the Department of Biomedical Engineering at Texas A&M University. His expertise is in optical sensing for diagnostic and biomedical monitoring applications. He is a fellow of four societies including SPIE, coauthor of over 300 publications, proceedings, patents, and abstracts, and cofounder of four medical device companies.